applied sciences

MDPI

Article

Optical Interband Transitions in Fully Strained $Ge_{1-x}Sn_x$ Alloys

Ping Tao *, Shaohan Li and Lijuan Wang

School of Electronic and Optical Engineering, Nanjing University of Science and Technology ZiJin College, Nanjing 210046, China; lishaohan1996@outlook.com (S.L.); zj_wanglj@163.com (L.W.)
* Correspondence: taoping@njust.edu.cn

Abstract

The optical transition characteristics of fully strained $Ge_{1-x}Sn_x$ films grown on Ge substrate were investigated by high-resolution X-ray diffraction (HRXRD) and spectroscopic ellipsometry (SE). The results showed Sn composition-dependent nonlinear behaviors in interband transition energies. The influence of strain on nonlinear behaviors was identified by the ratio of bowing parameters. Optical transition energies are largely tuned due to the strain-induced band structure. The strain in GeSn alloys may be responsible for the fluctuation of interband transition energies. The effect of full strain appears to result in an opposite trend in the direct and indirect band gap energies. The transition from indirect-to-direct band gap semiconductor in the present work is determined to be x = 0.103 at 300 K. These results contribute to further exploration into band gap engineering for mid-infrared optoelectronic materials.

Keywords: GeSn alloy; fully strained; interband transitions; high-resolution X-ray diffraction; spectroscopic ellipsometry

1. Introduction

Group VI elements are fascinating in assembling various compounds due to the attractive optical and electronic properties [1–3]. GeSn binary alloys are intriguing compounds and have been applied to optoelectronic devices [4–8]. A spectra range of 1.6 to 2.4 μm was obtained in GeSn μ-LEDs [7]. And high-speed GeSn resonance cavity-enhanced photodetectors present 2 μm band communication [8]. GeSn is an important infrared-emitting material. Expanding its spectra helps the development of optoelectronic devices. Although pure Ge is characterized by an indirect energy gap, $Ge_{1-x}Sn_x$ can be tuned to be a direct band gap semiconductor with a Sn composition of 3~17% [9–18]. The comparison between the direct and indirect energy gap determines the direct/indirect band gap semiconductors. Direct band gap GeSn with high quality was achieved [17]. The critical transition energy of indirect–direct (0.477 eV) was estimated by D'Costa et al. [11] Strain plays an important role in indirect–direct band gap transition as strain tunes the interband transition energies. Experiments showed that a compressive GeSn film has a direct band gap with a Sn content up to 17%, which is much larger than that of strain-free GeSn [13]. Also, theoretical investigation presented that tensile strain significantly impacts the band structure of GeSn [19]. The difference between the direct and indirect band gap energies can be reduced by tensile strain [20]. The photoluminescence of tensile-strained Ge moves to a longer wavelength as the in-plane tensile strain is increased [21]. The interband gap edge may be shifted as the strain develops in GeSn alloys. The application of strain-engineered GeSn in optoelectronic devices has been studied [22–25]. Strain induces changes in the energy band structure of

Check for updates

Academic Editor: Salvatore Gallo

Received: 16 March 2026
Revised: 6 June 2026
Accepted: 8 June 2026
Published: 13 June 2026

Copyright: © 2026 by the authors. Licensee MDPI, Basel, Switzerland. This article is an open access article distributed under the terms and conditions of the Creative Commons Attribution (CC BY) license.

GeSn. Large lattice mismatch between Ge and Sn makes it challenging to grow high-quality atomic bonding in GeSn. Both Sn composition and strain significantly influence the quality, the band gap structure, the optoelectronic properties, etc.

The interband transition energies are nonlinearly dependent on Sn composition. The Sn composition-dependent interband transition energies in GeSn alloys may be stated well by the bowing parameter b [9,11,12], which is important in materials design [11]. The bowing parameters for the direct band gap E_0 have mostly been reported [9,11,12,15,26–28]. And researchers have slightly discussed the bowing parameters for other interband transition energies: E_{ind}, E_1, $E_1 + \Delta_1$, E_0', E_2, respectively [11,12,15,29]. The values of the bowing parameters are smaller than 3 eV. The physics origination of the bowing parameters for GeSn alloys have been researched by groups. They found that bowing parameters are affected by atomic size, alloy disorder and electronegativity [11,12,29]. Detailed investigations of strain on GeSn interband transition energies and nonlinear behavior are still elusive. For fully strained GeSn films grown at low temperature, there are few reports on the transition of indirect to direct band gap.

In the present work, we investigate the effects of fully compressive strain on interband transition energies for GeSn films grown on Ge, including direct band gap energies, indirect band gap energies and other interband transition energies. Our results show that the influence of strain on interband transition energies may be indicated by the comparison of bowing parameters. The crossover concentration x from indirect to direct band gap for the $Ge_{1-x}Sn_x$ film has been determined by fitting the results of high-resolution X-ray diffraction.

2. Theory

Calculating lattice parameters helps to confirm the crystal's elastic state. The relaxed cubic lattice constant a_0 can be deduced from the measured in-plane lattice constant $a_{\parallel}$ and measured out-of-plane lattice constant $a_{\perp}$ according to Equations (1) and (2) [30]. The equations are written as the following formulas:

$$\frac{C_{12}}{C_{11}} = 0.3738 + 0.1676x - 0.0296x^2 \quad (1)$$

$$a_0 = (a_{\perp} + 2\frac{C_{12}}{C_{11}}a_{\parallel})/(1 + 2\frac{C_{12}}{C_{11}}) \quad (2)$$

The ratio of cubic elastic constants (C_{12}/C_{11}) is a compositional dependence for $Ge_{1-x}Sn_x$ alloys. The lattice constants a_0 are calculated based on measured lattice constants and the elastic constants.

GeSn alloys are important optical semiconductors and the transition from indirect band to direct band (IB-DB) is of vital interest. Although the data of spectroscopic ellipsometry cannot be supplied to investigate the indirect to direct band gap directly, we may do the calculations to determine the transition, which may be estimated by comparing the direct band gap energy to the indirect band gap energy. The band gap energies of strain-free GeSn alloys can be fitted by the formula [11–13,31]:

$$E(Ge_{1-x}Sn_x) = E_{Ge}(1-x) + E_{Sn}x - bx(1-x) \quad (3)$$

For the indirect band gap, b is 0.89 eV. And for direct band gap, b is 2.87 eV [31], which is consistent with that obtained by Gang He [9]. Also, the band edge of the GeSn alloy may

be shifted by the strain in the film. The conduction band and valence band for the fully strained GeSn alloys can be determined by the following equations [31]:

$$E_g = E(Ge_{1-x}Sn_x) + \Delta E_c + \Delta E_v \quad (4)$$

$$\Delta E_c = a_c(\varepsilon_{xx} + \varepsilon_{yy} + \varepsilon_{zz}) \quad (5)$$

$$\Delta E_v = b_v(\varepsilon_{xx} + \varepsilon_{yy} + \varepsilon_{zz}) + b_s(\varepsilon_{zz} - \varepsilon_{xx}) \quad (6)$$

Here, E_g represents the energy for the direct or indirect band gap. ΔE_c, ΔE_v are the band edge shift for both the conduction band and valence band induced by the strain. ε_{xx}, ε_{yy} represent the in-plane strain $\varepsilon_{\parallel}$. ε_{zz} represents the out-of-plane strain $\varepsilon_{\perp}$. a_c is the conduction band deformation potential. b_v, b_s are the valence band deformation potentials. The values of the strain are the same as above. These parameters come from Ref [31]. The values of a_c, b_v and b_s for $Ge_{1-x}Sn_x$ alloys are the result of linearly interpolating those of the two end materials, Ge and Sn, individually.

3. Experimental Details

Fully strained $Ge_{1-x}Sn_x$ films with Sn composition x = 0, 0.04, 0.08, and 0.14 were prepared on (004) Ge buffer by molecular beam epitaxy at National Taiwan University. The detailed grown parameters of the GeSn alloy films were described in our previous work [32]. Briefly, 30 nm GeSn films are grown on the 30 nm buffer Ge layer, which is deposited on the substrate Ge(004). The growth temperature is relatively low, set to 200 °C for both the Ge buffer layer and GeSn alloy films. The detailed strain states, thickness, and microstructures of GeSn alloys are determined by HRXRD, which is performed on the beamline BL14B1 located at the Shanghai Synchrotron Radiation Facility (SSRF) and the Beamline 1W1B at the Beijing Synchrotron Radiation Facility. The wavelength of the X-ray is chosen to be 1.238 Å and 1.54 Å, respectively. Optical properties are determined by SE at room temperature in the laboratory of Nanjing University. For SE measurement, which is carried out on an SE M-2000 produced by J.A. Woollam Co., Inc., 645 M Street, Suite 102, Lincoln, NE, USA, the incident angle is set to 65°. The acquisition of SE data requires the establishment of a hierarchical optical model. In this model, the parameters of each layer in the sample structure are the film thickness and optical constants. In the experiment, the Tauc–Lorentz oscillator approach was selected. Using an optical model and standard thin film equation rules, the SE data can be generated through software calculation. The measurement is in the range of 0.74 ∼ 5.1 eV with a step size of 0.01 eV.

4. Results

4.1. Fully Strained GeSn Alloys

The X-ray diffraction rocking curves for the GeSn films indicate that all alloy films are in full strain (epitaxy films) instead of relaxation [32]. Figure 1 shows the results of the HRXRD for the sample $Ge_{0.86}Sn_{0.14}$. Two reflections from the Ge substrate and $Ge_{0.86}Sn_{0.14}$ film are indicated in Figure 1a. In-plane and out-of-plane lattice parameters were deduced by the symmetric (004) and asymmetric (115) HRXRD. The diffraction of glancing incidence X-ray from different angles is presented in Figure 1b. The lattice constants of the film and the substrate are obtained and are consistent with each other. As is well known, the radius of a Sn atom is larger than that of a Ge atom and the larger lattice mismatch is up to 14.7% [27]. There may be an expansion in the GeSn alloy compared with crystal Ge due to Sn doping. The in-plane lattice compressive strain may induce out-of-plane lattice expansion, based on the elastic theory (tetragonal distortion). The in-plane lattice strain and out-of-plane lattice strain for our GeSn alloys are summarized and listed in Table 1.

The in-plane lattice strain is calculated by $\varepsilon_{\parallel} = (a_{\parallel} - a_{GeSn})/a_{GeSn}$ and the out-of-plane lattice strain is deduced by $\varepsilon_{\perp} = (a_{\perp} - a_{GeSn})/a_{GeSn}$. By comparison, we note that $\varepsilon_{\parallel}$ is larger than $\varepsilon_{\perp}$. $\varepsilon_{\parallel}$ is largely induced by the in-plane compressive Ge-Sn bond, while $\varepsilon_{\perp}$ is mainly induced by the tensile Ge-Ge bond in the growth direction. The strain $\varepsilon_{\parallel}$ is less than 0, on the contrary, which may be induced by misfit dislocation at the GeSn-Ge interface. $\varepsilon_{\perp}$ is larger than 0 and increases monotonically with increasing Sn composition. The Poisson ratio for $Ge_{1-x}Sn_x$ films is nonlinear dependence on Sn composition. The tensile Ge-Ge bonds are responsible for strain in the growth direction as the Sn composition is lower than 50% and Sn-Sn bond segregation exists. The cube roots of the volume are lower than the lattice constants deduced from Vegard's law in previous work [32]. The fully strained structure is compressive in our samples.

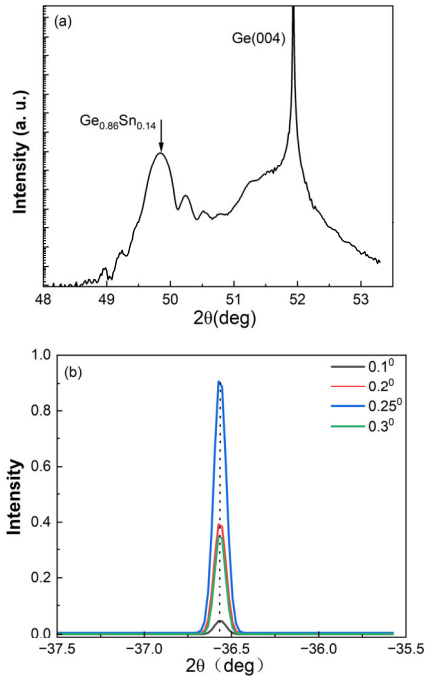

Figure 1. High-resolution X-ray diffraction patterns for $Ge_{0.86}Sn_{0.14}$/Ge alloy. (**a**) (004) symmetric reflection. (**b**) Glancing incidence diffraction at different angles. The dotted line indicates that these peaks have identical diffraction angles.

Table 1. In-plane, out-of-plane strain and lattice parameters for fully strained $Ge_{1-x}Sn_x$.

Sn Composition	$\varepsilon_{\parallel}$	$\varepsilon_{\perp}$	a_0	a_{vegard}
$x = 0.04$	−0.63%	0.46%	5.689	5.690
$x = 0.08$	−1.54%	1.03%	5.718	5.723
$x = 0.14$	−2.11%	1.85%	5.778	5.772

The elastic characteristics of the GeSn samples can be investigated by the strain above. The value a_{vegard} expresses the $Ge_{1-x}Sn_x$ lattice constant using Vegard's law, which is consistent with the strain-free lattice parameters a_0. The values a_0 and a_{vegard} for GeSn alloys are listed in Table 1. The result indicates that the fully strained structure for our GeSn samples is within the elastic range.

4.2. Ellipsometric Data Processing

The optical properties of GeSn alloys were measured by SE, and the complex dielectric function $\varepsilon_1 + i\varepsilon_2$ was obtained. Figure 2 presents the complex dielectric functions for bulk Ge and three $Ge_{1-x}Sn_x$ samples with Sn concentrations x = 0.04, 0.08 and 0.14. The spectra

focused on the energy range of 0.7–5.0 eV. The dielectric function spectra of GeSn show corresponding behavior to bulk Ge. The peaks of the real and imaginary parts for dielectric functions all appear at lower energies. The peak energies exhibit a significant redshift with increasing Sn content. These dielectric functions were adopted to further analyze interband transition energies for GeSn alloys.

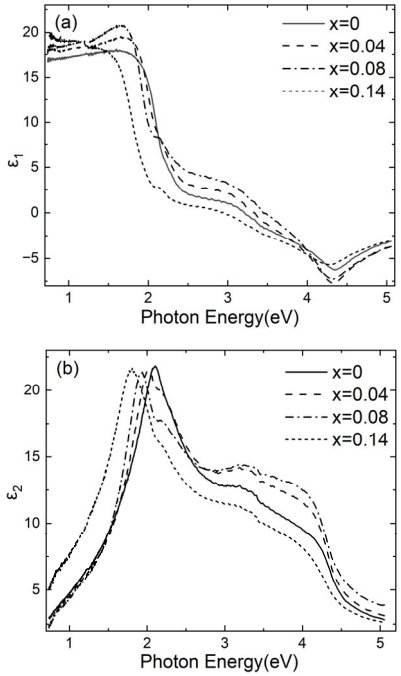

Figure 2. Infrared real and imaginary parts of the dielectric function for bulk Ge and $Ge_{1-x}Sn_x$ alloys with Sn concentration x = 0 (solid line), 0.04 (dash line), x = 0.08 (dash dot line), and x = 0.14 (short dash line). (**a**) Real part of the dielectric function; (**b**) Imaginary part of the dielectric function.

To obtain detailed analysis about interband transition energies, we smoothed the experimental data and calculated the second derivative of the imaginary part of the dielectric functions for $Ge_{1-x}Sn_x$ samples, as the raw imaginary spectra exhibited significant noise and irregular fluctuations. Figure 3 shows the second derivative of the imaginary part of the dielectric function for the $Ge_{0.86}Sn_{0.14}$ alloy and the line shape fitted with a two-dimensional saddle point [33–35]. The transition energies E_1, $E_1 + \Delta_1$, E_0', E_2 can be deduced from the fitting of the second derivative of ε_2 using the Savitzky–Golay method with Equation (7).

$$\frac{d^2\varepsilon}{d\omega^2} = \frac{Ae^{i\varphi}}{(\omega - E + i\Gamma)^2} \tag{7}$$

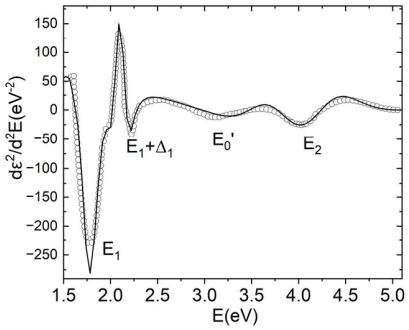

Figure 3. Second derivative of the imaginary part of dielectric function of $Ge_{1-x}Sn_x$ (x = 0.14) in solid line. The circles represent a fit with Equation (7).

The fitting contains four parameters (A amplitude, Γ the broadening of the critical points, E transition energy, and φ phase angle) for each point. The transition energies of the $Ge_{1-x}Sn_x$ samples were obtained by fitting the second-derivative curves of the imaginary parts. Then, the corresponding results presented in Table 2. The errors in energy estimation originate from dielectric function measurement, as well as the fitting. With rising Sn content, lattice mismatch between Ge and Sn atoms generates more dislocation defects within the GeSn alloy, which substantially increases measurement error.

Table 2. The transition energies (eV) for fully strained $Ge_{1-x}Sn_x$ alloys grown on Ge.

Sn Composition	E_1	$E_1+\Delta_1$	E_0'	E_2
$x = 0.04$	2.00 ± 0.02	2.25 ± 0.03	3.10 ± 0.03	4.25 ± 0.04
$x = 0.08$	1.91 ± 0.02	2.20 ± 0.03	3.06 ± 0.04	4.22 ± 0.05
$x = 0.14$	1.78 ± 0.04	2.18 ± 0.04	3.03 ± 0.06	4.04 ± 0.08

4.3. Critical Point Analysis

4.3.1. Direct and Indirect Band Gap Transitions

The direct and indirect band gap energies for strain-free and fully strained GeSn alloys have been estimated according to Equations (4)–(6). The calculated band gap energies decreased with increasing Sn composition. The direct band gap energy in our sample $Ge_{0.86}Sn_{0.14}$ is 0.393 eV, which is slightly larger than 0.328 eV and 0.330 eV in strain-free $Ge_{0.86}Sn_{0.14}$ alloy [10,36], while the indirect band gap energy (0.432 eV) is lower than that (0.473 eV) of strain-free alloy [10]. The full strain may be responsible for the energy difference. And the influence of the fully strained structure on the direct and indirect band gap energies is opposite for GeSn alloys. The ratios of fully strained band gap energies to strain-free ones are 1.08, 1.11, 1.39 and 0.989, 0.937, 0.906 for direct and indirect band gaps at x = 0.04, 0.08, 0.14, individually.

The Sn composition-dependent direct band gap energy is nonlinear. Figure 4 shows the nonlinear behavior of the direct band gap energy for fully strained GeSn alloys. The direct and indirect band gap energies for Ge and Sn are consistent with those reported by Tseng et al. [31]. It is interesting to know that the bowing parameter of fully strained GeSn alloys (2.02 eV) is lower than that of the strain-free alloys above, 2.87 eV. And for the indirect band gap, the bowing parameters are shown in Figure 5. The value is 1.14 eV for fully strained alloys, which is higher than that of strain-free alloys, 0.89 eV. The influence of full strain on bowing parameters for the direct and indirect band gap is just the contrary.

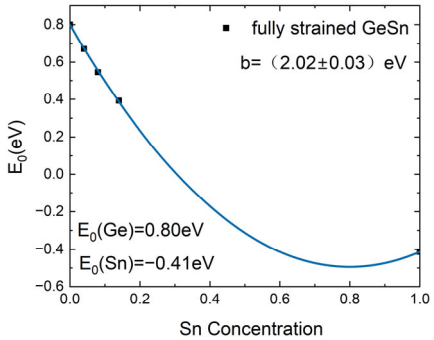

Figure 4. Sn composition-dependent direct band gap energies indicated by the bowing parameter at room temperature for fully strained GeSn alloys.

Figure 6 shows the IB-DB transition for fully strained GeSn alloys. The Sn composition for indirect to direct transition is 6.3% for strain-free GeSn alloys [12] and 17% for compressively strained GeSn/Ge(001) film with a growth temperature of 150 °C [13]. Compressive

strain induces an increase in the Sn composition for IB-DB to about 10.7% (from 6.3% to 17%). According to our result, while the Sn composition for strain-free alloys occurs at 5.5%, fully strained GeSn alloys may return to a direct band gap with a Sn composition up to 10.3% at room temperature. IB-DB transition energy is 0.487 eV, which is slightly larger than the result of GeSn films with a residual strain, 0.477 eV [11]. Compared with strain-free GeSn alloys, the bowing parameters for direct and indirect band gaps exhibit opposite behavior in fully strained samples. Therefore, the Sn composition for IB-DB transition is higher (from 0.55 to 1.03) than for strain-free GeSn alloys.

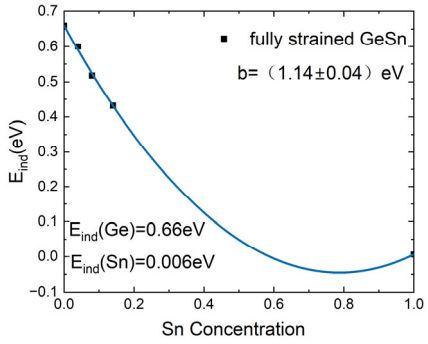

Figure 5. Sn composition-dependent indirect band gap energies indicated by the bowing parameter at room temperature for fully strained GeSn alloys.

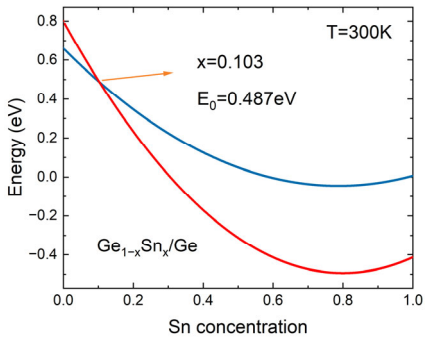

Figure 6. (Color online) Indirect band to direct band transition for fully strained GeSn alloys determined by the fitting at room temperature. The blue line shows the fitting of indirect band gap energies and the red line shows the fitting of direct band gap energies.

4.3.2. Four Interband Transitions

For GeSn alloys, the critical point energies are observed and decrease with increasing Sn composition. The transition energies E_1 for our GeSn alloys at x = 0.04, 0.08, and 0.14 are 2.00 eV, 1.91 eV, and 1.78 eV, respectively. The transition energies (1.91 eV and 1.78 eV) are slightly lower than those of strain-free GeSn films (1.99 eV and 1.84 eV) with Sn compositions of 0.08 and 0.14 [33]. For E_1 and E_2 points, the decreased transition energies for fully strained films are mostly lower than those of the strain-free GeSn alloys from Candi's work [33]. A similar trend is not observed at $E_1 + \Delta_1$ and E_0' critical points. The results indicate that the effect of fully strained structure varies at different critical points.

Figure 7 shows the fitting of transition energies E_1 using Equation (3). According to the fitting of E_1 from Candi's GeSn alloys, the value of the bowing parameter is 1.37 eV, which is close to 1.32 eV for the E_1 point [29]. The bowing parameter of the transition energy E_1 is 1.88 eV for fully strained GeSn alloys. Vijay's result shows that the bowing parameter of the E_1 point for strain-free GeSn alloys is 1.65 eV [11]. The comparison above shows that full strain in alloys increases the value of the bowing parameter of transition energies E_1.

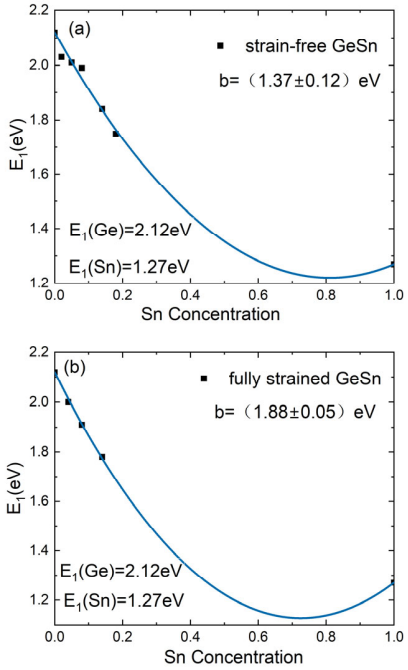

Figure 7. Compositional dependence of E_1 interband transitional energies: (**a**) strain-free GeSn alloys [33] and (**b**) fully strained GeSn alloys.

Figure 8 shows the compositional dependence of the $E_1 + \Delta_1$ transitions for $Ge_{1-x}Sn_x$ alloys. In Figure 8a, the transition energy $E_1 + \Delta_1$ for GeSn alloys is adopted from the reference [33]. The fits with Equation (3) show bowing parameters of 1.15 eV for strain-free $Ge_{1-x}Sn_x$ alloys and 0.53 eV for fully strained $Ge_{1-x}Sn_x$ alloys. The strain-free bowing parameter (1.15 eV) is slightly higher than the value of 1.05 eV reported in Ref. [11]. Full strain evidently reduces the bowing parameter of the GeSn alloy.

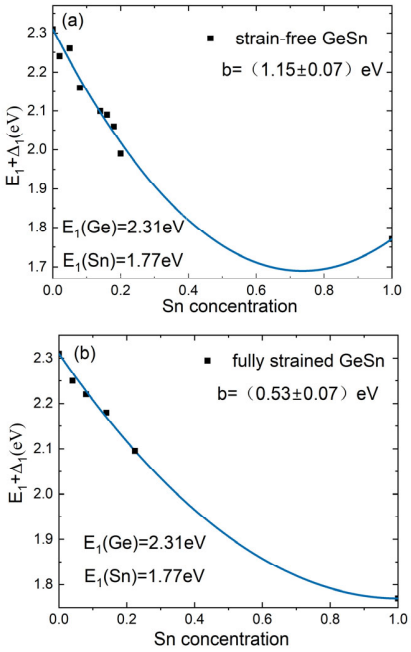

Figure 8. Compositional dependence of $E_1 + \Delta_1$ interband transitional energies: (**a**) strain-free GeSn alloys [33] and (**b**) fully strained GeSn alloys.

Figure 9 shows the fitting of transition energies E_0' using Equation (3). The bowing parameters are 0.17 eV and 0.09 eV, respectively. These bowing parameters are significantly

smaller than those at other critical points, indicating that these critical points are insensitive to structural strain in GeSn alloys.

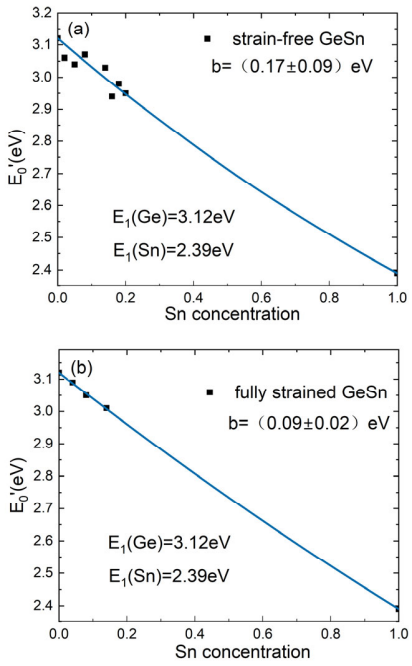

Figure 9. Compositional dependence of E_0' interband transitional energies: (**a**) strain-free GeSn alloys [33] and (**b**) fully strained GeSn alloys.

In Figure 10, we present the fitting of transition energies E_2 using Equation (3). The bowing parameter (0.66 eV) of strain-free GeSn is smaller than that (1.65 eV) of fully strained GeSn alloys for the E_2 critical point. The trend for the E_2 point is different from the critical points $E_1 + \Delta_1$, E_0'. The significant difference between the strain-free and fully strained bowing parameters may arise from the smoothing of experimental data.

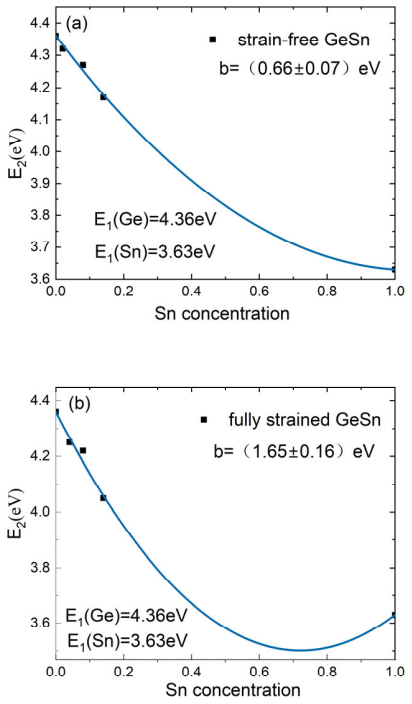

Figure 10. Compositional dependence of E_2 interband transitional energies: (**a**) strain-free GeSn alloys [33] and (**b**) fully strained GeSn alloys.

5. Discussion

To analyze the nonlinear behavior of Sn composition-dependent interband energies, the bowing parameters of GeSn alloys are summarized in Table 3. Table 3 concerns the bowing parameters for E_0, E_{ind}, E_1, $E_1+\Delta_1$, E_0', E_2 critical points. The average bowing parameters are presented to investigate the strain-induced nonlinear behavior. The bowing parameters of the transition energies E_0, E_{ind}, E_1, $E_1+\Delta_1$, E_0', E_2 for our samples have been indicated above. The bowing parameters of the direct band gap E_0 for strain-free and strained GeSn alloys are reported mostly by researchers [9,11,12,15,26–28]. We calculated the average bowing parameters for the strained E_0 point (2.20 eV), which is lower than that of strain-free GeSn alloys (2.72 eV) from the references above. For the E_{ind} point, the average bowing parameter of strained GeSn alloys (1.09 eV) is lower than that of strain-free alloys (0.86 eV) [11,29]. The difference of bowing parameters between strained and strain-free alloys (1.60 eV vs. 1.51 eV) is small for the E_1 point. For the $E_1+\Delta_1$, E_0', E_2 points, the transition energies of our GeSn alloys are shown in Table 2. We referred to the literature and obtained these bowing parameters [11,29]. The strained and strain-free bowing parameters are 0.82 eV, 0.37 eV, and 1.03 eV and 1.10 eV, 0.33 eV, and 0.53 eV for $E_1+\Delta_1$, E_0', E_2, respectively. The ratios of strained bowing parameters to strain-free ones are shown in Table 3.

Table 3. Bowing parameters (b) for strained (b_s) and strain-free ($b_{s\text{-}f}$) GeSn alloys.

b/eV	E_0	E_{ind}	E_1	E_1+Δ_1	$E_0^{'}$	E_2
b_s	2.20	1.09	1.60	0.82	0.37	1.03
$b_{s\text{-}f}$	2.72	0.86	1.51	1.10	0.33	0.53
Ratio	0.81	1.27	1.06	0.75	1.12	1.94

In Table 3, the ratios of the E_0, E_{ind}, $E_1+\Delta_1$, E_2 critical points significantly deviate from the value of 1. The effect of strain on the bowing parameters for the E_1, E_0' points is confirmed to be minor since the ratios are close to 1. For the E_0, E_{ind} critical points, the band structure is related to the center of the Brillouin zone [37]. The Brillouin zone center of GeSn exhibits high intrinsic symmetry, which can be broken by the lattice strain in the crystal. Strain in GeSn alloys disrupts the structural balance and induces fluctuations in interband transition energies.

6. Conclusions

We have detected the nonlinear behavior of interband transition energies in fully strained GeSn films grown by molecular beam epitaxy. The bowing parameters for the direct and indirect band gaps of fully strained GeSn alloys are 2.02 eV and 1.14 eV, respectively. The ratios of strained to strain-free bowing parameters indicate that strain significantly affects the critical points' energies and induced fluctuation. The original balance may be disturbed by strain in GeSn alloys. The transitional Sn composition of the indirect to direct band gap for our fully strained GeSn alloys is located at x = 0.103 at room temperature.

Author Contributions: Conceptualization, P.T.; Methodology, S.L.; Software, L.W.; Validation, P.T. and S.L.; Writing—original draft preparation, P.T. and L.W.; Writing—review and editing, P.T. All authors have read and agreed to the published version of the manuscript.

Funding: This research was funded by the Natural Science Foundation of the Jiangsu Higher Education Institutions of China, grant number 24KJD510006 and Nanjing University of Science and Technology Zijin College "High-End Talent Aggregation" Research Initiation Project, grant number 2024ZK0003.

Data Availability Statement: The original contributions presented in this study are included in the article. Further inquiries can be directed to the corresponding author.

Acknowledgments: We thank beamline BL14B1 (Shanghai Synchrotron Radiation Facility) and BSRF (Beijing Synchrotron Radiation Facility) for providing the beam time. And We also express special gratitude to National Taiwan University and Nanjing University for providing experimental support. The suggestions from the relevant editors and reviewers have improved the quality of this paper, and we would like to express our sincere gratitude to them.

Conflicts of Interest: The authors declare no conflicts of interest.

References

1. Kang, S.; Kil, Y.H.; Park, B.G.; Choi, C.J.; Kim, T.S.; Jeong, T.S.; Shim, K.H. Optical Properties of $Si_{1-x}Ge_x$ Quantum Dots Grown using RPCVD. *Electron. Mater. Lett.* **2011**, *7*, 121–125. [CrossRef]
2. Gallagher, J.D.; Xu, C.; Senaratne, C.L.; Aoki, T.; Wallace, P.M.; Kouvetakise, J.; Menendez, J. $Ge_{1-x-y}Si_xSn_y$ light emitting diodes on silicon for mid-infrared photonic applications. *J. Appl. Phys.* **2015**, *118*, 135701. [CrossRef]
3. Zhang, Q.; Liu, Y.; Yan, J.; Zhang, C.; Hao, Y.; Han, G. Theoretical investigation of tensile strained GeSn waveguide with Si_3N_4 liner stressor for mid-infrared detector and modulator applications. *Opt. Express* **2015**, *23*, 7924–7932. [CrossRef]
4. Tseng, H.H.; Li, H.; Mashanov, V.; Yang, Y.J.; Cheng, H.H.; Chang, G.E.; Soref, R.A.; Sun, G. GeSn-based p-i-n photodiodes with strained active layer on a Si wafer. *Appl. Phys. Lett.* **2013**, *103*, 231907. [CrossRef]
5. Stange, D.; Driesch, N.; Zabel, T.; Armand-Pilon, F.; Rainko, D.; Marzban, B.; Zaumseil, P.; Hartmann, J.M.; Ikonic, Z.; Capellini, G.; et al. GeSn/SiGeSn Heterostructure and Multi Quantum Well Lasers. *ACS Photonics* **2018**, *5*, 4628–4636. [CrossRef]
6. Atalla, M.R.M.; Lemieux-Leduc, C.; Assali, S.; Koelling, S.; Daoust, P.; Moutanabbir, O. Extended short-wave infrared high-speed all-GeSn PIN photodetectors on silicon. *APL Photonics* **2024**, *9*, 056103. [CrossRef]
7. Liu, X.; Huang, Q.; Zheng, J.; Cui, J.; Zhu, Y.; Yang, Y.; Liu, Z.; Zuo, Y.; Cheng, B. GeSn μ-LED Array with Programmable Spectra for Near-Infrared Microspectrometer. *ACS Photonics* **2025**, *12*, 1220–1226. [CrossRef]
8. Cui, J.; Zheng, J.; Zhu, Y.; Liu, X.; Wu, Y.; Huang, Q.; Yang, Y.; Liu, Z.; Liu, Z.; Zuo, Y.; et al. High-speed GeSn resonance cavity enhanced photodetectors for a 50 Gbps Si-based 2 μm band communication system. *Photonics Res.* **2024**, *12*, 767–773. [CrossRef]
9. He, G.; Atwater, H.A. Interband Transitions in Sn_xGe_{1-x} Alloys. *Phys. Rev. Lett.* **1997**, *79*, 1937–1940. [CrossRef]
10. Perez Ladron de Guevara, H.; Rodriguez, A.G.; Navarro-Contreras, H.; Vidal, M.A. Determination of the optical energy gap of $Ge_{1-x}Sn_x$ alloys with $0 < x < 0.14$. *Appl. Phys. Lett.* **2004**, *84*, 4532.
11. D'Costa, V.R.; Cook, C.S.; Birdwell, A.G.; Littler, C.L.; Canonico, M.; Zollner, S.; Kouvetakis, J.; Menéndez, J. Optical critical points of thin-film $Ge_{1-y}Sn_y$ alloys: A comparative $Ge_{1-y}Sn_y/Ge_{1-x}Si_x$ study. *Phys. Rev. B* **2006**, *73*, 125207. [CrossRef]
12. Yin, W.-J.; Gong, X.-G.; Wei, S.-H. Origin of the unusually large band-gap bowing and the breakdown of the band-edge distribution rule in the Sn_xGe_{1-x} alloys. *Phys. Rev. B* **2008**, *73*, 161203. [CrossRef]
13. Tonkikh, A.A.; Eisenschmidt, C.; Talalaev, V.G.; Zakharov, N.D.; Schilling, J.; Schmidt, G.; Werner, P. Pseudomorphic GeSn/Ge(001) quantum wells: Examining indirect band gap bowing. *Appl. Phys. Lett.* **2013**, *103*, 032106. [CrossRef]
14. Gupta, S.; Magyari-Köpe, B.; Nishi, Y.; Saraswat, K.C. Achieving direct band gap in germanium through integration of Sn alloying and external strain. *J. Appl. Phys.* **2013**, *113*, 073707. [CrossRef]
15. Jiang, L.; Gallagher, J.D.; Senaratne, C.L.; Aoki, T.; Mathews, J.; Kouvetakis, J.; Menéndez, J. Compositional dependence of the direct and indirect band gaps in $Ge_{1-y}Sn_y$ alloys from room temperature photoluminescence: Implications for the indirect to direct gap crossover in intrinsic and n-type materials. *Semicond. Sci. Technol.* **2014**, *29*, 115028. [CrossRef]
16. Wang, X.; Chen, C.; Feng, S.; Wei, X.; Li, Y. A hybrid functional first-principles study on the band structure of non-strained $Ge_{1-x}Sn_x$ alloys. *Chin. Phys. B* **2017**, *26*, 127402. [CrossRef]
17. Li, Y.-L.; Huang, Z.-M.; Huang, W.-Q.; Liu, S.-R. Direct bandgap transition for emission in GeSn nanowires. *Nanotechnol. Rev.* **2025**, *14*, 20250215. [CrossRef]
18. Gunder, C.; de Oliveira, F.M.; Wangila, E.; Stanchu, H.; Zamani-Alavijeh, M.; Ojo, S.; Acharya, S.; Said, A.; Li, C.; Mazur, Y.I.; et al. The growth of Ge and direct bandgap $Ge_{1-x}Sn_x$ on GaAs (001) by molecular beam epitaxy. *RSC Adv.* **2024**, *14*, 1250–1257. [CrossRef]
19. Zhang, Q.; Liu, Y.; Yan, J.; Zhang, C.; Hao, Y.; Han, G. Simulation investigation of tensile strained GeSn fin photodetector with Si_3N_4 liner stressor for extension of absorption wavelength. *Opt. Express* **2015**, *23*, 739–746. [CrossRef]
20. Lieten, R.R.; Seo, J.W.; Decoster, S.; Vantomme, A.; Peters, S.; Bustillo, K.C.; Haller, E.E.; Menghini, M.; Locquet, J.P. Tensile strained GeSn on Si by solid phase epitaxy. *Appl. Phys. Lett.* **2013**, *102*, 052106. [CrossRef]
21. Jakomin, R.; de Kersauson, M.; El Kurdi, M.; Largeau, L.; Mauguin, O.; Beaudoin, G.; Sauvage, S.; Ossikovski, R.; Ndong, G.; Chaigneau, M.; et al. High quality tensile-strained n-doped germanium thin films grown on InGaAs buffer layers by metal-organic chemical vapor deposition. *Appl. Phys. Lett.* **2011**, *98*, 091901. [CrossRef]
22. Buca, D.; Bjelajac, A.; Spirito, D.; Concepción, O.; Gromovyi, M.; Sakat, E.; Lafosse, X.; Ferlazzo, L.; von den Driesch, N.; Ikonic, Z.; et al. Room Temperature Lasing in GeSn Microdisks Enabled by Strain Engineering. *Adv. Opt. Mater.* **2022**, *10*, 2201024. [CrossRef]

23. Chuang, Y.; Liu, C.; Luo, G.; Li, J. Electron Mobility Enhancement in GeSn n-Channel MOSFETs by Tensile Strain. *IEEE Electron Device Lett.* **2021**, *42*, 10–13. [CrossRef]
24. Elbaz, A.; Buca, D.; von den Driesch, N.; Pantzas, K.; Patriarche, G.; Zerounian, N.; Herth, E.; Checoury, X.; Sauvage, S.; Sagnes, I.; et al. Ultra-low-threshold continuous-wave and pulsed lasing in tensile-strained GeSn alloys. *Nat. Photonics* **2020**, *14*, 375–382. [CrossRef]
25. Burt, D.; Zhang, L.; Jung, Y.; Joo, H.J.; Kim, Y.; Chen, M.; Son, B.; Fan, W.; Ikonic, Z.; Tan, C.S.; et al. Tensile strained direct bandgap GeSn microbridges enabled in GeSn-on-insulator substrates with residual tensile strain. *Opt. Lett.* **2023**, *48*, 735. [CrossRef] [PubMed]
26. Mathews, J.; Beeler, R.T.; Tolle, J.; Xu, C.; Roucka, R.; Kouvetakis, J.; Menéndez, J. Direct-gap photoluminescence with tunable emission wavelength in $Ge_{1-y}Sn_y$ alloys on silicon. *Appl. Phys. Lett.* **2010**, *97*, 221912. [CrossRef]
27. Chibane, Y.; Ferhat, M. Electronic structure of Sn_xGe_{1-x} alloys for small Sn compositions: Unusual structural and electronic properties. *J. Appl. Phys.* **2010**, *107*, 053512. [CrossRef]
28. Lin, H.; Chen, R.; Weisheng, L.; Yijie, H.; Kamins, T.I.; Harris, J.S. Investigation of the direct band gaps in $Ge_{1-x}Sn_x$ alloys with strain control by photoreflectance spectroscopy. *Appl. Phys. Lett.* **2012**, *100*, 102109. [CrossRef]
29. Xu, C.; Senaratne, C.L.; Kouvetakis, J.; Menéndez, J. Compositional dependence of optical interband transition energies in GeSn and GeSiSn alloys. *Solid-State Electron.* **2015**, *110*, 76–82. [CrossRef]
30. Beeler, R.; Roucka, R.; Chizmeshya, A.V.G.; Kouvetakis, J.; Menéndez, J. Nonlinear structure-composition relationships in the $Ge_{1-y}Sn_y$/Si(100) ($y < 0.15$) system. *Phys. Rev. B* **2011**, *84*, 035204.
31. Tseng, H.H.; Wu, K.Y.; Li, H.; Mashanov, V.; Cheng, H.H.; Sun, G.; Soref, R.A. Mid-infrared electroluminescence from a Ge/$Ge_{0.922}Sn_{0.078}$/Ge double heterostructure p-i-n diode on a Si substrate. *Appl. Phys. Lett.* **2013**, *102*, 182106. [CrossRef]
32. Tao, P.; Huang, L.; Cheng, H.H.; Wang, H.-H.; Wu, X.-S. Epitaxial growth of $Ge_{1-x}Sn_x$ films with x up to 0.14 grown on Ge (00l) at low temperature. *Chin. Phys. B* **2014**, *23*, 088112. [CrossRef]
33. Cook, C.S.; Zollner, S.; Bauer, M.R.; Aella, P.; Kouvetakis, J.; Menendez, J. Optical constants and interband transitions of $Ge_{1-x}Sn_x$ alloys ($x < 0.2$) grown on Si by UHV-CVD. *Thin Solid Film.* **2004**, *455*, 217–221.
34. Viña, L.; Logothetidis, S.; Cardona, M. Temperature dependence of the dielectric function of gerriianium. *Phys. Rev. B* **1984**, *30*, 1979. [CrossRef]
35. Lautenschlager, P.; Garriga, M.; Vina, L.; Cardona, M. Temperature dependence of the dielectric function and interband critical points in silicon. *Phys. Rev. B* **1987**, *36*, 4821. [CrossRef]
36. Pérez Ladrón de Guevara, H.; Rodríguez, A.G.; Navarro-Contreras, H.; Vidal, M.A. Nonlinear behavior of the energy gap in $Ge_{1-x}Sn_x$ alloys at 4 K. *Appl. Phys. Lett.* **2007**, *91*, 161909. [CrossRef]
37. Bauer, M.R.; Cook, C.S.; Aella, P.; Tolle, J.; Kouvetakis, J.; Crozier, P.A.; Chizmeshya, A.V.G.; Smith, D.J.; Zollner, S. SnGe superstructure materials for Si-based infrared optoelectronics. *Appl. Phys. Lett.* **2003**, *83*, 3489. [CrossRef]

Disclaimer/Publisher's Note: The statements, opinions and data contained in all publications are solely those of the individual author(s) and contributor(s) and not of MDPI and/or the editor(s). MDPI and/or the editor(s) disclaim responsibility for any injury to people or property resulting from any ideas, methods, instructions or products referred to in the content.